

Article

Light Intensity of Phosphorescent-Netting Pots and Determining Their Visibility to Snow Crab (*Chionoecetes opilio*) Using Visual Modeling Techniques [†]

Colin Frank ^{1,*} , Shannon Bayse ^{1,2} , Riognach Steiner ¹ and Pierre-Paul Bitton ² 

¹ Centre for Sustainable Aquatic Resources (CSAR), Marine Institute, Memorial University of Newfoundland, St. John's, NL A1C 5S7, Canada; shannon.bayse@mi.mun.ca (S.B.); riognach.steiner@mi.mun.ca (R.S.)

² Cognitive and Behavioural Ecology (CABE), Memorial University of Newfoundland, St. John's, NL A1C 5S7, Canada; pbitton@mun.ca

* Correspondence: colin.frank@mi.mun.ca; Tel.: +1-709-778-0583

[†] This manuscript is part of the Master thesis by the first author Colin Frank, available online at <https://research.library.mun.ca/16302/1/converted.pdf> (accessed on 10 May 2024).

Abstract: This study explores the visibility of phosphorescent-netting pots to snow crab (*Chionoecetes opilio*) using visual modeling techniques. Light emitted from such pots increases catch per unit effort, yet little is understood about the factors driving these higher catch rates. In this study, we measure pot light emission and snow crab visual acuity. Combining these data with estimates obtained in the literature for other biotic and abiotic factors, we model snow crab vision in relation to the pots. Utilizing these factors and environmental conditions, we derive a contrast ratio between the pot light and the ambient light. Findings reveal that the visibility of pot lights at 200-m depth depends primarily on solar angle (time of day) and time elapsed post-deployment. Additional factors influencing the vision of the pots include water column quality and benthic boundary layer turbidity. This study is the first to model the visual ecology of snow crab and the first to estimate snow crab visual acuity. These insights into snow crab visual ecology can potentially enhance fishing techniques, promote catch efficiency and sustainability, and help provide a path forward for visual ecology research in the fisheries science field.

Keywords: visual ecology; fishing technology; visual acuity; strontium aluminate; phosphorescence

Key Contribution: This study pioneers the understanding of the visual ecology of snow crab, which is an important international fisheries species.



Citation: Frank, C.; Bayse, S.; Steiner, R.; Bitton, P.-P. Light Intensity of Phosphorescent-Netting Pots and Determining Their Visibility to Snow Crab (*Chionoecetes opilio*) Using Visual Modeling Techniques. *Fishes* **2024**, *9*, 185. <https://doi.org/10.3390/fishes9050185>

Academic Editor: Darrell Mullowney

Received: 28 March 2024

Revised: 10 May 2024

Accepted: 14 May 2024

Published: 17 May 2024



Copyright: © 2024 by the authors. Licensee MDPI, Basel, Switzerland. This article is an open access article distributed under the terms and conditions of the Creative Commons Attribution (CC BY) license (<https://creativecommons.org/licenses/by/4.0/>).

1. Introduction

The commercial snow crab fishery is Newfoundland and Labrador's most economically important fishery, bringing over \$761 million to the province in a \$1.37 billion industry sector [1]. However, as Mullowney et al. [2] attest, sustainably managing the fishery does not come without substantial difficulties. The bycatch of animals other than snow crab is not a significant issue in this fishery, so management focuses on minimizing non-marketable snow crab (soft-shell, undersized [carapace width, CW, <95 mm], and female), all of which must be discarded at sea [3]. The Newfoundland snow crab fishery currently uses gear (pots) designed to be size-selective, thereby minimizing the catch of female and undersized male snow crab by controlling mesh size [3]. Thus, small individuals can escape through the mesh while the larger crab are unable to escape and are retained. However, the bycatch of soft-shell snow crab, which is too large to escape through the mesh, can only be mitigated through control efforts such as area and fishery closures. Reducing soft-shell snow crab bycatch is essential, as it can sometimes comprise more than 50% of the total catch, and 15–20% is generally needed to close an area to fishing [2,3]. Discarding snow

crab contributes to fishing mortality and harms the snow crab population by reducing current and future spawning stock biomass and, in effect, recruitment [3]. Reducing total bycatch and discards while maintaining comparable landings would help fishers and assist management in maintaining sustainability [4].

Although regulating mesh size proves to be effective in removing female and undersized snow crab, the average soak time in the Newfoundland and Labrador snow crab fishery is three to five days [5], while the optimal soak time allowing undersized snow crab to escape is around nine days [6]. Controlling soak time from a management perspective is challenging to enforce. The disjunction between optimal soak time for the fishery and optimal soak time for undersized crab escape highlights the need for additional gear design if the fishery wishes to improve catch efficiency by increasing catch per unit effort (CPUE) and decreasing bycatch.

The governing body that manages snow crab fisheries in Newfoundland and Labrador, Fisheries and Oceans Canada (DFO), employs a proactive strategy to minimize bycatch of soft-shell snow crab by starting the fishing season in the spring when the soft-shell snow crab catch-to-target ratio is at its lowest [3]. This timeline allows researchers and the industry to help minimize soft-shell catches by improving catch efficiency. However, individual quotas are often not met until summer, when the soft-shell catch ratio increases [2]. Increasing the CPUE may fill individual quotas before soft-shell catches dramatically increase. Additionally, a higher CPUE potentially reduces fishing time at sea, thereby cutting fuel costs, carbon footprints, and opportunities for work-related injuries [7].

There have been many attempts to create a more efficient pot in global snow crab fisheries [8–10]. Most new pot designs focus on changing the shape, the escape opening size/shape, or the entrance of the pot [8,9,11]. Recently, changes employed the use of light in conjunction with bait in an attempt to create an additional form of positive taxis (movement toward light) [4,7] in theory (currently the mechanism behind snow crab catch rates increasing with light use is unknown). Fishers have historically used bait (squid, fish, etc.) as a means to attract crabs to pots, initiating a dynamic behavior between chemotaxis and rheotaxis, or attraction through chemical means and against the current, respectively [12,13]. In the case of chemotaxis, crabs are only attracted to the pot if they initially come into contact with the chemicals from the bait (bait plume), which are subject to ocean currents and diminish over time and distance [12]. When another form of positive taxis is used, such as light or sound (phototaxis or phonotaxis), an even dispersion of stimuli is projected from the pot in all directions, potentially attracting crab without being subject to currents [4]. Thus far, the two forms of light explored in the snow crab fishery are light-emitting diodes (LEDs) and phosphorescence [7,14], and both light forms increased CPUE. LEDs are currently too expensive to use on a commercial scale due to the combination of the cost of the lights, batteries, and replacement of lost components while fishing. Replacing dead or dying batteries with new or newly charged batteries also adds to the fishing time and may increase marine litter. Conversely, purchasing phosphorescent netting for a pot is cheaper than purchasing and maintaining LEDs for industry-standard netting, and it recharges within minutes of sunlight exposure [14]. In those regions where sunlight is seasonally limited (e.g., Alaska and Norway), there is an option to quickly charge the netting using ultra-violet (UV) lights [14]. However, using UV lights does add to the cost and complications of using phosphorescent-netting pots.

Luminescent materials, generally those that emit light without heat, consist of both phosphorescent and fluorescent materials. When fluorescent materials are excited by a source of radiation, generally UV light, the material immediately releases lower wavelength light. Fluorescent materials cease to glow after the radiation source is removed. Phosphorescent materials, such as the type used in the snow crab fishery, absorb energy from a light source and trap that energy, allowing it to continuously emit lower-wavelength light for a certain amount of time. Recent advances in phosphorescent technology have led to various applications in the last two decades [15]. Historically, sulfide-based phosphorescence is the most common source of industrial glowing material. It is known to be a

low-intensity and quickly dissipating light source, severely limiting its potential. However, in 1996, europium and dysprosium (Eu^{2+} and Dy^{3+}) rare-earth-element-doped strontium aluminate expanded the possible use of luminous material. The new phosphorescent material is roughly 10 times brighter and lasts 50 times longer than commercial sulfur-based phosphorescence [16]. Using UV light, Fouzar et al. [17] found that the charge time of strontium aluminate, depending on its exact composition, is generally less than 10 s and decreases in cold temperatures, with greater than 90% of a full charge within milliseconds of UV exposure when at 14 °C. Other elements can be used with strontium aluminate with varying degrees of light intensity and decay [17,18].

In this study, we use pots with strontium aluminate-based phosphorescent twine (referred to as phosphorescent-netting pots; also referred to as luminescent-netting pots in the literature), as they are currently the most economically feasible method of using light commercially. The drawback to using phosphorescent-netting pots is that when they are removed from a high-intensity light source (UV, sunlight) the emitted light intensity exponentially decreases, as opposed to the long-lasting LEDs [14]. Our goal in this study was to understand the visual abilities of snow crab and how they perceive phosphorescent-netting pots in commercially relevant depths, water qualities, and distances, which is currently unknown. Once the limitations of the gear are known in respect to snow crab vision, how best to employ them in the fishery can be considered.

To understand how snow crab may see phosphorescent-netting pots, it is important to understand how abiotic factors influence vision in the ocean, including depth, water quality, distance from the object, ambient light, and phosphorescent duration (light intensity over time). Fortunately, these are all well-studied variables, and we can make reasonable assumptions and develop ranges for each [19–21]. However, it is also important to understand the visual capabilities of snow crab (acuity, spectral sensitivity, and contrast threshold), and no studies, to our knowledge, provide such information. This data deficit does not make it impossible to make inferences, as there have been many vision studies on different species of crustaceans [20,22,23]. Meyers et al. [24] indicated that snow crab possess apposition compound eyes, allowing us to make more informed assumptions within those data gaps.

In this study, we aim to understand the visual capabilities of snow crab, in general, and concerning phosphorescent-netting pots. To understand those interactions and capabilities, we (1) characterize the light emitted from the phosphorescent material in the pots (intensity and decay); (2) determine the abiotic characteristics of the relevant fishing environment from the existing literature (ambient light over time, water quality, depth, and turbidity); (3) measure snow crab visual acuity; (4) determine other visual characteristics of snow crab using the existing literature (contrast and spectral sensitivity); and (5) model the photon flux and Michelson contrast ratio of phosphorescent-netting pots in snow crab eyes using the results from objectives 1–3.

2. Materials and Methods

2.1. Light Characteristics of Phosphorescent Twine

We used three different intensities of phosphorescent twine, each manufactured by Euronete (Euronete company, Maia, Portugal). All three treatment types (2-strand, 4-strand, and 6-strand) had a different number of phosphorescent fibers woven in with standard polyethylene strands. The first and dimmest treatment has only two glowing strands and is also the only netting that is commercially available for snow crab pots. The second and third treatments are woven with four and six glowing strands, respectively. All pots were Japanese-style conical pots with a bottom diameter of 102 cm, top diameter of 55.5 cm, height of 44 cm, and mesh size of 135 mm.

To determine the spectral irradiance from the twine, we glued twine from each treatment to individual cardboard discs (radii = 6.0 cm) in a tight spiral pattern to create 100% coverage on each disc. There were five replicates per treatment, and each replicate's light was measured three times. Discs were placed in a sunlit environment for at least one hour

before measurements were taken. They were quickly taken to a dark room one disc at a time and placed in a fixed location. We used the Ocean Optics QE Pro spectrometer (Ocean Insight, Orlando, FL, USA) to measure the relative and absolute irradiance of the glowing twine across the visible spectrum (400–700 nm). The QE Pro spectrometer is designed for low-light applications because of its minimized noise (signal-to-noise ratio 1000:1), high optical resolution (~1.2 nm), and wide range of wavelengths (~185–1100 nm). Relative irradiance is the measure of power across the electromagnetic spectrum and can be helpful when comparing the light intensity of different sources or when interested in the spectral curve of an object or light source. Absolute irradiance is more challenging to obtain and is the measure of the number of photons emitted at each wavelength from an object or light source, which thoroughly describes its spectral characteristics. For absolute irradiance measurements, the cosine corrector CC-3-UV-S was used, and the spectrometer was calibrated using the Ocean Optics DH-3P-CAL light source. While relative irradiance measurements were taken for all treatments, absolute irradiance was only taken for the brightest treatment, the 6-strand treatment, and was extrapolated for the 2- and 4-strand treatments using the results from the relative irradiance measurements. For example, if the relative irradiance of the 4-strand is 50% of the 6-strand, then the absolute irradiance of the 6-strand would be multiplied by 0.50 and assumed to be the absolute irradiance of the 4-strand. We used five replicates of 6-strand twine to measure the decay rate, taking relative irradiance measurements with 5 min integration times for 60 min. Because the phosphorescent twine is composed of the same material in each treatment, we assumed the decay rates of the 2- and 4-strand treatments were the same as the 6-strand treatment, given that they are composed of the same materials; the decay rate is influenced by the composition of the material and not its quantity. After taking light measurements, the distance between the disk and the receiver was measured and recorded to account for light lost between the disc and the cosine corrector.

We first collected the data from the spectrometer using OceanView software, version 2.0.15 (Ocean Insight). The spectral data were then analyzed using R software, version 4.4.0 [25] and pavo, a spectral analysis package [26]. The absolute brightness of the 6-strand treatment was initially measured in $\mu\text{W}/\text{cm}^2/\text{nm}$ with a 5 min integration time but was converted to photons/ $\text{m}^2/\text{nm}/\text{s}$ by using the conversion formula $((\text{irradiance} \times 10^{-6}) \times 10^4)/300 \times \text{wavelength} \times 5.05 \times 10^{15}$ [27]. Relative irradiance measurements from each replicate were averaged. From the relative irradiance measurements, absolute values were then calculated for the two other treatments, 4- and 2-strand. Correction factors for the distance from the receiver to the disc were implemented using SACALC3 software, version 1.4 [28] (settings are given in Appendix A).

The light decay was modeled using a standard power law decay function (Equation (1)) that was previously used in strontium aluminate studies [17,29]. Parameters were fitted to the measured decay data using a negative log-likelihood function and the `optim()` function from the base R stats package [25].

$$I_t = S \cdot t^{-\alpha} \quad (1)$$

2.2. Snow Crab Visual Characteristics

2.2.1. Visual Acuity

We removed the left and right eyes from three commercially legal adult male snow crab ($\text{CW} \geq 95$ mm) during the Newfoundland commercial fishing season to estimate snow crab visual acuity. Soft, female, and undersized male snow crab were not sampled because they are considered bycatch and must be discarded at sea [3]. Eyes were immediately placed in 10% neutral buffered formalin. We then took images of the eyes under a dissecting microscope and measured interommatidial distance, roughly the diameter of each facet, using ImageJ software, version 1.53e [30]. We selected eight locations across the eyes for measurements owing to varying facet sizes: forward distal, forward middle, forward proximal, middle distal, middle middle, middle proximal, rear distal, and rear middle (Figure 1A). Distal and proximal are named according to the eyestalk's attachment

site. Fifteen measurements were taken per location per eye and averaged across individuals. Using ImageJ, circles were fitted to the images to determine local area curvature [22,31] (see the Supplementary Materials). Curvature was measured in the vertical axis of the eye (slightest curvature); thus, the results could be considered to be the vertical resolving power (Figure S1). Using Equation (2), we determined the distance that the light from the pot may fall on a single ommatidium, becoming a point source of light. The model distance limitations (before an object becomes a point source) were determined by measuring interommatidial angles in all eight regions of the snow crab eyes; to achieve this, we divided the interommatidial distance ($\Delta\theta$) by the radius of the local area curvature of the eye (R). Next, we divided the smallest measurement of the commercial pot (height = $O = 440$ mm) and solved for the maximum sighting distance (U) [32]. This method results in a best-case scenario and may slightly overestimate visual acuity. However, it is an acceptable alternative for acuity estimation without additional physiological studies determining snow crab eyes' focal lengths, acceptance angles, and presence or absence of neural pooling [33,34]. Lastly, we used the R package AcuityView [35] to visualize the spatial resolution of snow crab when viewing a phosphorescent-netting pot from several distances. A photograph of the 6-strand pot was taken using a 12 MP camera and was resized to a resolution of 2048×2048 pixels for processing. The pot was resized within the photographs to simulate a distance perspective along with the decreased resolution that comes with distance. Only the highest and lowest acuity estimates were used when predicting the resolution of the pots. Human vision of the pots was also processed to illustrate the acuity of snow crab.

$$\Delta\theta = D/R = O/U \quad (2)$$

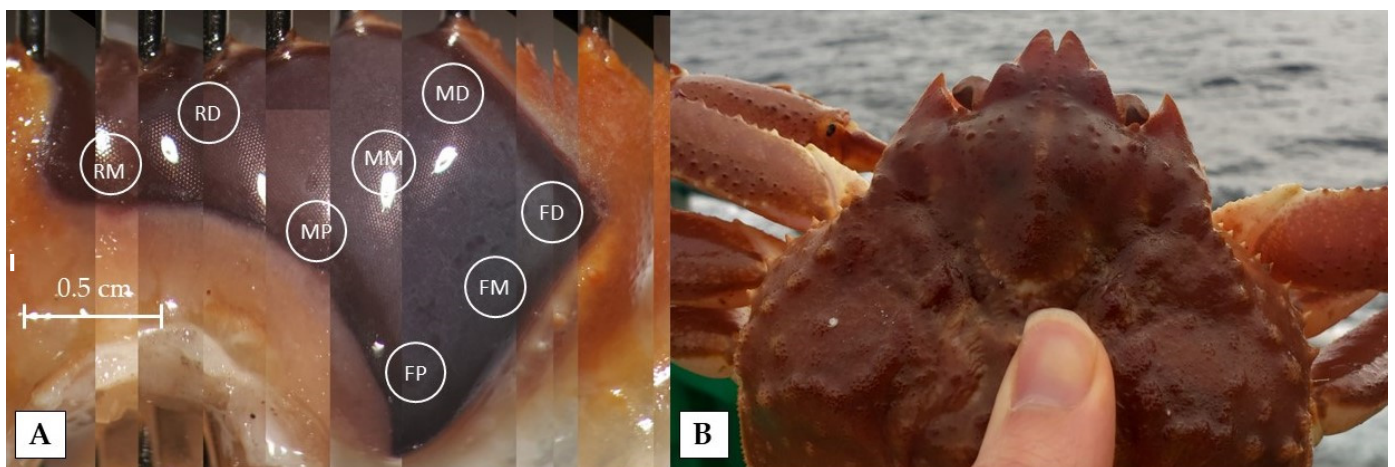


Figure 1. (A) A composited picture of a snow crab eye under a dissecting microscope. White circles indicate acuity measurement locations. The area on the right is front-facing on a live snow crab, and the left is rear-facing. The bottom is proximal, and the top is distal. Regions are labeled rear middle (RM), rear distal (RD), middle proximal (MP), middle middle (MM), middle distal (MD), forward proximal (FP), forward middle (FM), and forward distal (FD). (B) The rear ommatidia wrap around the back of the eye and face dorsally when the eyestalks are positioned against the body wall, as in the picture, but are facing posterolaterally on the horizon when eyestalks are in the elevated position.

2.2.2. Spectral Sensitivity

To our knowledge, the spectral sensitivity of snow crab has not been documented. However, most crabs that have been studied have a single visual pigment in photoreceptor cells 1–7, which follows a standard sensitivity distribution with a maximum between 473 nm (blue) and 515 nm (green) [23]. Although many shallow-water crustaceans have a photoreceptor cell eight that can detect UV light, this area of research is lacking. In this study, we assume that UV light is not present in the fishing environment; therefore, we

can restrict our focus to those photoreceptor cells that are sensitive to longer wavelengths. When focusing on crabs more closely related to snow crab or who have similar life histories, a sensitivity of roughly 495 nm is the most likely maximum spectral sensitivity of snow crab [23,36,37]. Following recommendations from previous research [23,38], we chose to model the snow crab spectral sensitivity to a general sensitivity function for vitamin A₁-based visual pigments, Dartnall's nomogram [39]. To incorporate Dartnall's nomogram, a by-hand measuring tool into the model, we used a polynomial function (Equation (3)) to describe snow crab spectral sensitivity [38]. The function describes the log absorption coefficient (B) per wavelength (λ) using peak absorption of vitamin A₁-based visual pigments (L_{max}) and the estimated snow crab spectral shift in peak absorption (λ_{max}). Additional parameters for the polynomial function can be found in the Supplementary Materials.

$$B(\lambda) = \sum_{k=1}^8 b_k \left[\left(\frac{L_{max}}{\lambda} \right) - \left(\frac{L_{max}}{\lambda_{max}} \right) \right]^k \quad (3)$$

2.2.3. Contrast Sensitivity (Michelson Contrast)

We used a Michelson contrast sensitivity function to determine if snow crab could distinguish the phosphorescent netting from the ambient light. We chose to use Michelson contrast because it is more appropriate when modeling the visibility of patterns within an object, as light from around the patterns can obscure the image [20]. The Michelson contrast ratio in our model ranges from 0 to 1. The farther the contrast value is from 0, the more likely the object is visible, with the minimum contrast threshold being the point at first detection. We also chose a range of minimum contrast thresholds (high = 0.10, medium = 0.15, low = 0.20) in which snow crab could likely distinguish the phosphorescent light from ambient light. We selected a range because the contrast sensitivity of snow crab is unknown. However, based on limited research on the contrast sensitivity of decapods, this range (0.10 to 0.20) is an appropriate approximation for a low-light environment [40]. Contrast thresholds are not a static number and vary with ambient light and temperature [41], which is especially important when considering animals that migrate between shallow and deep water. However, we only considered a single range because we assumed a static fishing environment at 200 m.

2.3. Pot Viewed at Depth by Snow Crab

2.3.1. Light from the Pot Area

To estimate the total light from the pot, light from the twine was added to the horizontal ambient light from the spaces between the twine. We achieved this by using ImageJ to quantify the proportion of the pot area composed of twine when viewed horizontally (P). We then multiplied the phosphorescent twine measurements (L_{gt}) by the proportion of twine coverage in Equation (4). We applied diffuse attenuation coefficients per wavelength per meter (e^{-Kd}) to estimate light loss due to scattering and absorption for each water type [42] (see Section 2.4.1 for water types used). The space between the twine (1 - P) was multiplied by the background irradiance (L_{bz}) (Equation (5)), known as veiling light [43], and added to Equation (4) as the total irradiance from the pot area [27,44]. A correction factor for solar angle was added to the background irradiance (∠) to estimate the amount of light available at any time during the day calculated for every 10 min between sunrise and sunset and interpolated for each minute between the 10-min calculations. At night, between sunset and sunrise, ∠ was a constant multiplier reducing the ambient light by six orders of magnitude from solar noon [27].

$$L_{gt} \times e^{-Kd} \times P \quad (4)$$

$$L_{bz} \times (1 - P) \times \angle \quad (5)$$

2.3.2. Solid Angle

We account for the size and distance of the pot by converting it to a solid angle as perceived by a snow crab. Solid angles, measured in steradians, are dimensionless units that are included in the model to adjust for the apparent decrease in the size of the pot to the surrounding environment. By definition, the pot's solid angle decreases exponentially as the distance from the snow crab eye increases and vice versa [27]. The solid angle (Ω_g) is equal to the area of the pot as seen from the side (A_g) divided by the distance squared (d^2) from the snow crab eye to the pot (Equation (6)).

$$\Omega_g = \frac{A_g}{d^2} \quad (6)$$

2.4. Environmental Conditions Affecting Viewing

2.4.1. Ambient Light Intensity and the Spectral Curve

In this study, to model the impact of water properties on light propagation, we used the Jerlov water quality classification system [21], which was first described for oceanic water and then expanded to productive coastal waters. The system describes the irradiance transmissibility of different water types. The water types are, in order from clear to turbid: Jerlov I, IA, IB, II, III, 1C, 3C, 5C, 7C, and 9C [42]. The snow crab fishery between Conception Bay, Newfoundland, and Labrador, Canada, was used as an example location for measurements (Lat: 47.5850, Long: -53.2134). Water-quality estimates in this region range between Jerlov I and 1C waters [45]. Therefore, we used Jerlov I, III, and 1C water qualities to predict the scattering and absorption properties of coastal and oceanic Newfoundland waters. Ambient light values (horizontal radiance) for Jerlov water types I and III at 200 m (109 fms) deep were used from published data [46] and converted into irradiance by multiplying by pi [27,44]. The ambient light values were adjusted according to the solar angle from when the measurements were taken (68.6°) and local solar noon (53.4°) [27] (p. 45). The spectral curve for Jerlov type I waters at 200 m was estimated from measurements by Johnsen et al. [47]. However, spectral curves for Jerlov type III and 1C waters are not known and were instead estimated using diffuse attenuation coefficients [42] and surface light data derived from SMARTS v2.9.5 Fortran code [48] (settings are given in Appendix A). To model how the time of day affects the snow crab's ability to see the phosphorescent-netting pots, we determined the proportion of light available outside of solar noon according to the solar angle at each minute and adjusted the ambient light accordingly [27] (p. 45). Ambient light during the night (after 19:57) was estimated to be six orders of magnitude lower than that of solar noon [27].

2.4.2. Turbidity in the Benthic Boundary Layer

We estimated the impact of benthic boundary layer (BBL) turbidity on the visual models in Jerlov type III waters, as it most accurately represents coastal Newfoundland [31]. To estimate the effect of turbidity, the diffuse attenuation coefficients (K in Equation (4)) from the phosphorescent twine were changed to match turbid waters (Jerlov 3C = medium turbidity, Jerlov 9C = high turbidity). In effect, we assume that the ambient light level is maintained, but the light from the pot does not travel as far in moments or areas of increased turbidity in the BBL.

2.5. Photon Flux and Michelson Contrast

Combining the measurements from Equations (1) and (3)–(6), along with the area of the average facet in the highest acuity region of the eye (m^2), we modeled the total photon flux (Φ), that is, the amount of light reaching the retina of a snow crab that is produced by the pot (Equation (7)). Using the same values and equations, the background photon flux (Equation (8)) was modeled. Both photon flux measurements, Φ_{gt} and Φ_{bz} , were used to determine the Michelson contrast (C) (Equation (9)). Additional parameters added were the

average facet area in the highest acuity region of the eye (A_{sc}) and the sensitivity function (f) results from Equation (3).

$$\Phi_{gt} = \left((L_{gt} \times e^{-Kd} \times P) + (L_{bz} \times (1 - P) \times \angle) \right) \times \Omega_g \times A_{sc} \times f \quad (7)$$

$$\Phi_{bz} = (L_{bz} \times (1 - P) \times \angle) \times \Omega_g \times A_{sc} \times f \quad (8)$$

$$C = \frac{\Phi_{gt} - \Phi_{bz}}{\Phi_{gt} + \Phi_{bz}} \quad (9)$$

3. Results

3.1. Phosphorescent Twine Characteristics

The visible spectrum in all three treatment groups follows the same distribution and peaked at 523 nm (green). Relative measurement results show that light intensity at this wavelength jumps 2.3-fold from 2-strand to 4-strand twine, while it only increases an additional 1.8-fold from 4-strand to 6-strand twine, totaling about a 4.2-fold increase in intensity from 2-strand to 6-strand twine.

The absolute intensity measurements of the 6-strand twine resulted in a photon emission of (at 21 °C) 2.7×10^{13} q/m²/s across all wavelengths between 400 and 700 nm. When we apply the absolute intensity results of the 6-strand twine to the relative measurements of 4-strand and 2-strand twine, as described above, we obtain 1.5×10^{13} q/m²/s and 6.4×10^{12} q/m²/s, respectively. The peak wavelength in the absolute intensity measurement was the same as the relative measurement (523 nm). At the peak wavelength, 6-, 4-, and 2-strand light emission was 3.7×10^{11} , 2.1×10^{11} , and 9.6×10^{10} q/m²/s (Figure 2).

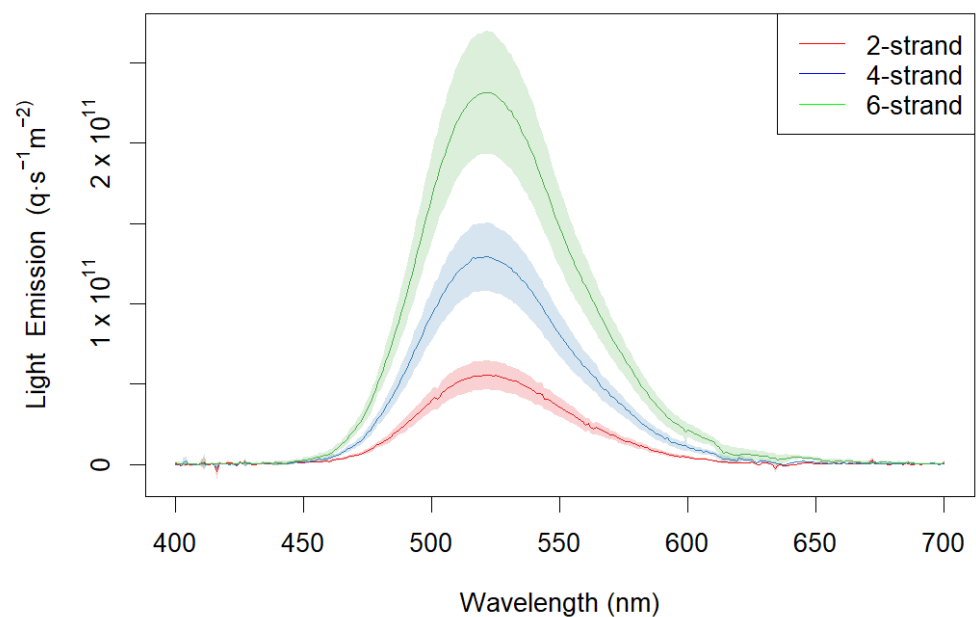


Figure 2. Absolute intensity measurements of the 6-strand phosphorescent twine and the extrapolated 4-strand and 2-strand measurements according to relative intensity measurements.

The optimized negative log-likelihood function produced decay results of $S = 1.06$ and $\alpha = 1.16$ for Equation (1). Decay rates show that initial intensity is reduced dramatically within the first 10 min and begins to reach an asymptotic-like stage after 30 min (Figure 3A). The decay rate results in Figure 3B show that the initial decay rate had a 54% reduction in light intensity after the first five min but was reduced to 36% following the next five-minute interval. With increasing time, the decay rate per five-minute interval began to reach an asymptote-like stage with increasing deviation around the mean.

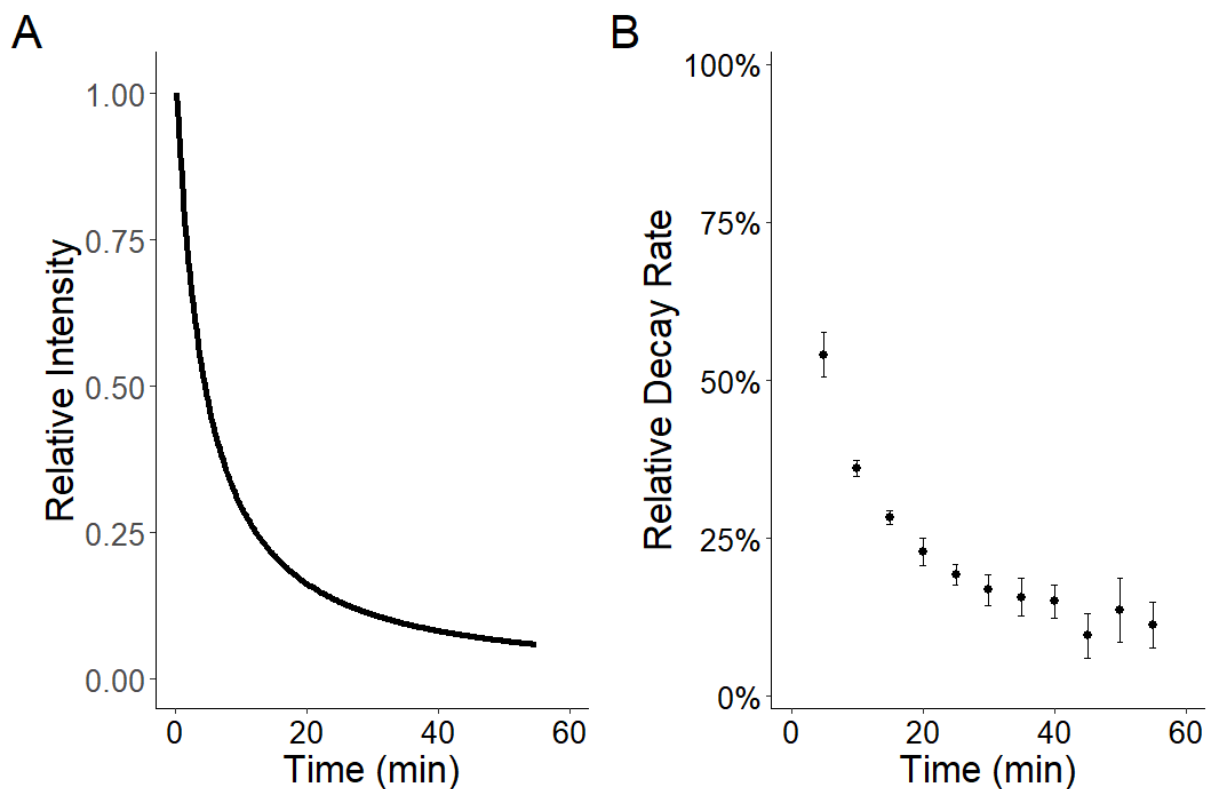


Figure 3. Phosphorescent-twine intensity decay results over time. (A) The optimized exponential model derived from the decay results. (B) The percent decay rate relative to the preceding measurement. Error bars indicate the standard deviations of results across replicates.

3.2. Snow Crab Visual Acuity Measurements

Visual acuity results vary across the snow crab eye, with the greatest resolution in the forward-facing and middle parts of the eye (Table 1). The distal portions of the eye had the worst acuity, as there was more curvature in these measured locations. Although the rear-facing ommatidia had the largest facets, visual acuity was moderate because the curvature was slight. The AcuityView-produced images (Figures 4 and 5) illustrate the limitations of snow crab visual acuity, as blurry light sources begin to dissipate and blend with the background. The images are created using the highest and lowest acuity values from Table 1.

Table 1. Adult male (carapace width ≥ 95 mm) snow crab inter-ommatidial measurements with standard deviations and corresponding acuity-related derivations: D = Distal, M = Middle, P = Proximal. R = Radius of curvature, $\Delta\theta$ = Interommatidial angle, U = maximum sighting distance of phosphorescent-netting pots.

Measurement	Front D.	Front M.	Front P.	Mid D.	Mid M.	Mid P.	Rear D.	Rear M.
Mean (mm)	0.057	0.061	0.060	0.067	0.071	0.059	0.076	0.076
SD (mm)	0.004	0.003	0.003	0.003	0.003	0.004	0.004	0.005
R (mm)	1.2	3.8	2.2	1.5	3.7	1.1	1.2	2.8
$\Delta\theta$ (rad)	0.048	0.016	0.027	0.045	0.019	0.054	0.063	0.027
U (m)	9.2	27.4	16.2	9.9	23.1	8.2	7.0	16.3

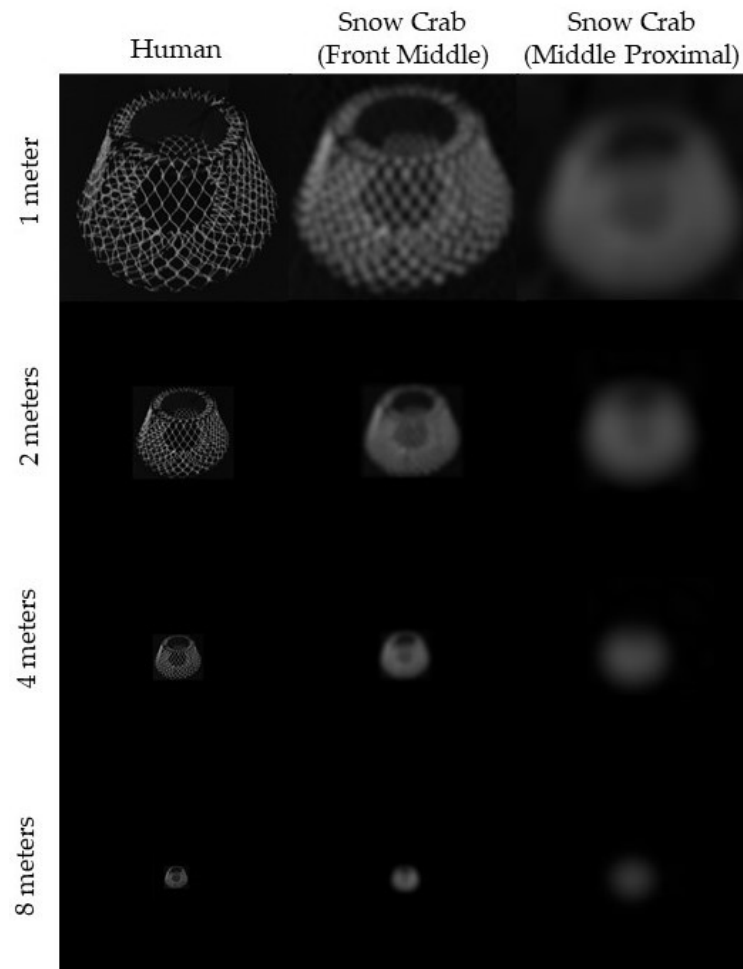


Figure 4. A monochromatic picture of a 6-strand phosphorescent-netting pot in a dark environment simulating the acuity of a human eye and a snow crab eye in the zone with highest acuity (front middle) and the zone with lowest acuity (middle proximal). Pictures scaled to highlight perspective. Light and contrast sensitivity are not accounted for in these images. Figure created using the AcuityView package in R.

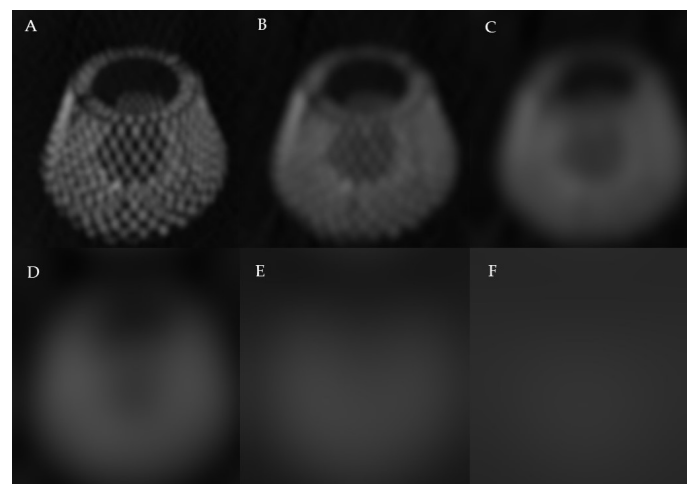


Figure 5. A monochromatic picture of a 6-strand phosphorescent-netting pot in a dark environment simulating the highest acuity of snow crab (front middle) at (A) 1 m, (B) 2 m, (C) 4 m, (D) 8 m, (E) 16 m, and (F) 30 m. Pictures not scaled to highlight the resolution of the pot. Figures created using the AcuityView package in R.

3.3. Contrast of Phosphorescent Light in Different Water Types

The models estimate that light from all three phosphorescent-netting pot treatments is not distinguishable from ambient light to snow crab at 200 m in clear oceanic water during the minimum solar zenith. However, in coastal waters (Jerlov III and 1C), the light from the phosphorescent-netting pots becomes increasingly visible as the number of phosphorescent strands within the twine increases (Figure 6). Turbidity models from Jerlov III waters show that increased turbidity affects the sighting distance more than it does the decay (Figure 7), changing the y-intercept (distance) while the x-intercept (time) remains relatively unchanged. Lastly, the extended time models show if the pots are dropped in the evening, the distance the light from the pot is visible increases dramatically after sunset (Figure 8).

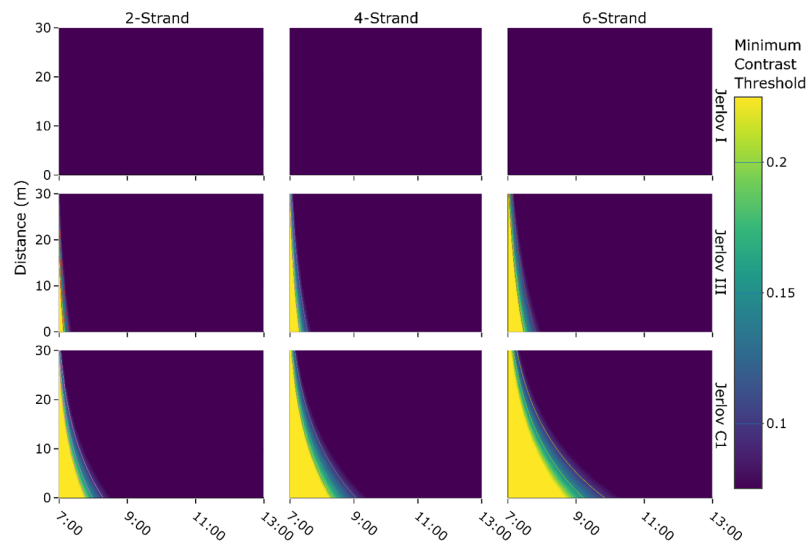


Figure 6. Snow crab visual contrast plots for each phosphorescent-netting pot treatment (columns) and three water types (rows). Models are set at 07:00 on 18 April 2022, in Conception Bay, NL (Solar angle = 8°). The y-axis is the distance from the pot to the eye of a snow crab, and the x-axis is the time from pot deployment when light emission intensity begins to decay and solar angle increases. Colors indicate Michelson contrast values: yellow = visible, green and light blue = possibly visible, and dark blue = not visible.

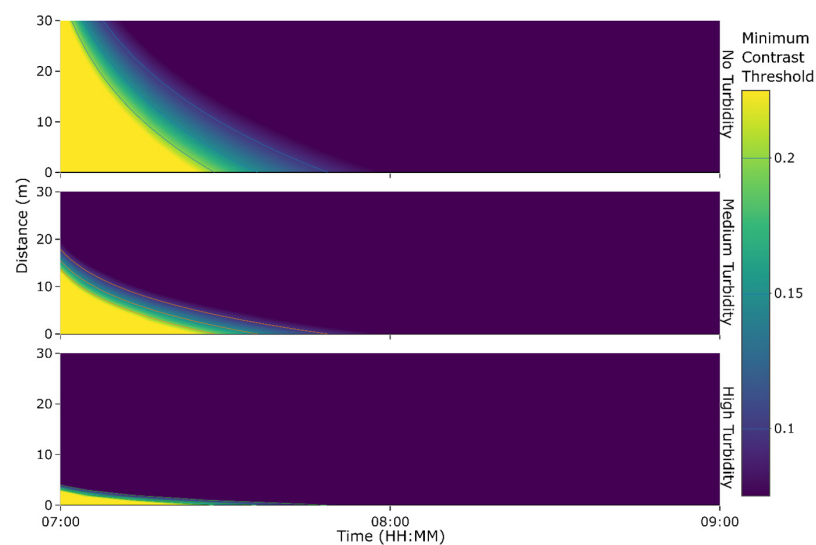


Figure 7. Snow crab visual contrast plots for 6-strand pots in three benthic boundary layer turbidity scenarios. Each scenario is simulated at 07:00 (NT) in Conception Bay, NL, on 18 April 2022. Models are all set within Jerlov III waters. Colors indicate Michelson contrast values: yellow = visible, green and light blue = possibly visible, and dark blue = not visible.

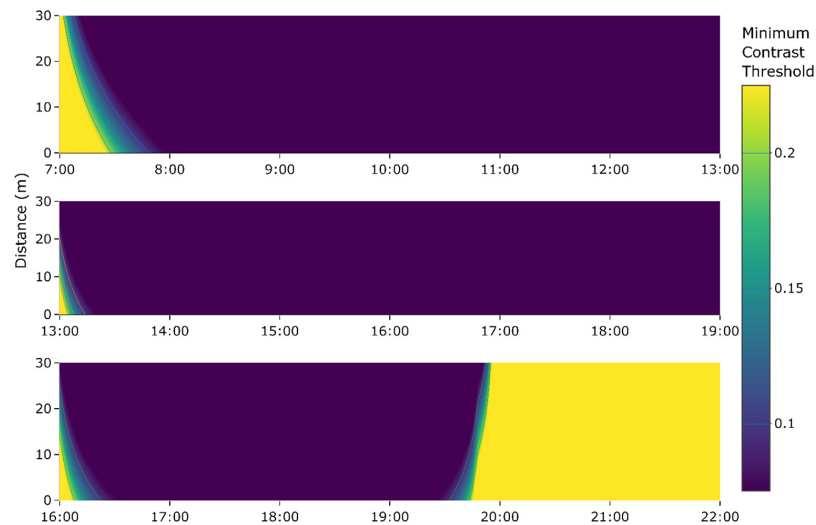


Figure 8. Snow crab visual contrast plots for 6-strand phosphorescent-netting pots at three different setting times (solar angle): 07:00–13:00 NT (8° to 53.4°), 13:00–19:00 NT (53.4° to 8.5°), and 16:00–22:00 NT (37.8° to -18.77°), Conception Bay, NL, 18 April 2022. Models are all within Jerlov III waters. Colors indicate Michelson contrast values: yellow = visible, green and light blue = possibly visible, and dark blue = not visible.

4. Discussion

4.1. Main Factors Influencing the Visibility of Light from Phosphorescent-Netting

The results from this study show that the main factor that influences the visibility of phosphorescent-netting pots is the amount of ambient light at depth, which is under constant change, depending mainly on the solar angle, but it is also determined by water column absorption and scattering properties [42,49]. This is all dependent on deployment time, as pot light intensity rapidly decreases once set. In addition to solar angle, water column quality, and deployment time, other factors that contribute to an ever-changing underwater light environment are cloud coverage, wave height and periodicity, suspended sediment, plankton layers, phytoplankton concentration, and anthropogenic light [49–51]. The results help us better understand the prominence of solar irradiance at 200 m and its effect on the diurnal behavior of the animals that live in this environment. Though the light at these depths is only a fraction of the solar irradiance at the surface, there is enough light to mask low-intensity light throughout much of the day.

4.2. Strontium Aluminate Properties

Models were not extrapolated beyond six hours because (1) the manufacturer claims that the twine is visible for a minimum of six hours if fully charged, (2) slight errors in the decay rate could affect the contrast models significantly, as the model predicts further beyond the 60 min that was measured, and (3) our decay model appears asymptotic, which assumes that emitted light never reaches zero. Because we did not take measurements beyond 60 min, we cannot say that the emitted light never reaches zero beyond those six hours. As seen in Figure 3B, the increase in variance around the measurements indicates that the light levels begin to reach a lower limit for the optical spectrometer and there is likely some noise influencing the readings. This increase in variance prompted us to limit extended predictions in light availability beyond measured values. Regardless, at such low light levels, the contrast model may not be appropriate at these times, and even if the pot is brighter than the surrounding light, it may be too dim to stimulate the visual system [52] (i.e., there may not be enough photons to stimulate a visual response; see the Supplementary Materials).

Studies suggest that the most efficient temperature for strontium aluminate's phosphorescence is 65 °C, much warmer than ocean water temperatures, and efficiency is reduced when it is colder or warmer [17]. Personal observations indicated little difference between the decay rates in phosphorescent twine from room (21 °C) to cold (−2 °C) temperatures. This deviation from previous studies on strontium aluminate is likely due to it being mixed within a polymer, thereby affecting its absorption and emission properties. Strontium aluminate and polymer composites have significantly reduced light intensity and slowed decay rates [53,54]. However, studies, to our knowledge, have not tested temperature effects on the emission properties, such as long-term decay rates, of strontium aluminate/polymer composites.

4.3. Visibility of Phosphorescent Netting in Different Conditions

The only commercially available phosphorescent-netting pot in the Newfoundland and Labrador fishery, the 2-strand, is hardly visible to snow crab in Newfoundland-type waters (Jerlov III) during peak sunlight hours, significantly limiting the potential benefits of the light emission during this time. When the solar angle is low, the sighting distance is drastically diminished when medium or heavy turbidity is simulated in the BBL currents (Figure 7). Pots may be deployed after the maximum solar angle (about mid-day) to increase the contrast between the pots and the ambient light (Figure 8). Setting the pots at dusk would take advantage of the dramatic decrease in ambient light levels while emitting a significant amount of phosphorescent light in later hours, maximizing the contrast between the two light sources. Another way to further increase the contrast is to charge pots using UV lights on the boat before a night deployment. However, we cannot say a higher contrast would catch more snow crab without knowing why snow crab enter lit pots at higher rates. On the contrary, research suggests that the 4-strand pots outperform 6-strand pots with a 12% increase in adult male snow crab catch [55], suggesting that light attraction may be more nuanced than brighter means better.

4.4. Snow Crab Visual Characteristics and Their Environment

Acuity measurements suggest that beyond 27.4 m in the front-facing middle portion of the eye (Table 1), the light from phosphorescent-netting pots will fall on a single ommatidium and become a point source of light. These results show that snow crab have relatively high visual acuity compared with other crustaceans, likely enabled by their larger size, allowing them to carry large compound eyes. With large compound eyes, snow crab can have large facets for low-light sensitivity and a small interommatidial angle for higher resolution. The model does not go beyond 30 m, because point sources of light require additional complexities that are not within the bounds of these models. With that in mind, if a pot were visible beyond this maximum distance as a point source, its visibility would decrease dramatically with increasing distance as the ambient light began taking more space within the single ommatidium. Each ommatidium acts to sample a region of space for average brightness rather than complexity [20]. With decreasing brightness in a single ommatidium, the phosphorescent light would eventually be discounted as noise during neural processing [20]. The perceived brightness, or radiance, of a light source is generally conserved in the air or in a vacuum until it becomes a point source, which becomes dimmer according to the inverse square law ($\text{intensity} = 1/\text{distance}^2$). Underwater, the inverse square law is compounded by light scattering and absorption [27]. Regardless, there is little chance that a single point source of dim light, such as those beyond that 27.4 m, would be visible and affect the behavior of a snow crab due to a myriad of visual phenomena (e.g., noise, diffraction) [20,32].

When crabs enter a defensive "sitting" position, their eyes are generally situated within the orbital space (Figures 1B and 9) to protect them from damage or to appear less conspicuous by tucking in both legs and eyes [56,57]. Juvenile snow crab and tanner crab (*Chionoecetes bairdi*) fully or partially bury themselves as a primary defensive response to predators, likely retracting their eyes to remain inconspicuous [58,59]. Crabs can still

visualize and react to their environment when their eyes are in the orbital space, though many of their ommatidia face either the ground or the body wall. In this position, the dorsal-facing part of the eye is composed of large ommatidia (Figure 10), which are commonly seen in benthic and pelagic crustaceans with predators or prey that approach from above. The large facets increase light sensitivity for better spotting silhouettes against dim downwelling light [20,60]. The interommatidial angle is slightly larger in the dorsal-facing part of the eye, reducing the resolving power compared with the forward and middle sections. The increased light sensitivity in the dorsal-facing part of the eye when in a defensive, sitting, or buried position is likely a tactic to scan above for the silhouettes of predators while remaining inconspicuous. In this position, the ability of snow crab to see phosphorescent-netting pots is likely poor, due in part to the lower number of ommatidia scanning the horizon and the increased terrain obstruction when positioned low to the seafloor.



Figure 9. Snow crab pseudopupil. Images are from the eye's forward and ventral facing areas when in the orbital space. They are anteromedial to anterolateral facing when elevated, scanning the horizon. The pseudopupil is vertical when the eyes are elevated.

When the eye is not situated in the orbital space, it is elevated; the distal portion is dorsal, and the proximal portion is ventral. The front is still front-facing (anteromedial), and the rear is still rear-facing (posterolateral), but both are scanning the horizon instead of facing forward and dorsal. In the elevated position, the distal area of the eye has a thin set of ommatidia with poor resolution that may view directly above. The small interommatidial angle in the middle section of the eye falls in line with other crustaceans that need better vertical spatial resolution, where they can scan the horizon for predators near the seafloor while also looking for their next meal, a potential mate, or to see point-source bioluminescence from a greater distance [20,60,61]. This characteristic can be compared to the fiddler crab, *Gelasimus vomeris*, which also lives in a flat environment. Fiddler crabs respond to any object above the horizon as a potential threat, as might snow crab [62]. Above the horizon, fiddler crabs are wary of birds, while snow crab are preyed upon by

large fish and marine mammals [3,63]. Snow crab have most of their ommatidia focused on the horizon for better spotting conspecifics and food, while ommatidia facing above spot predators and those below help determine the distance of benthic structures or other animals [62]. These areas also have smaller facets compared with the posterolateral area and likely come at the cost of reduced light sensitivity. Because most of the ommatidia are focused on the horizon and acuity slightly increases from the mediolateral to posterolateral parts of the eye, snow crab can likely see pots directly in front of them the best, with or without additional light. However, the increased facet size in the posterolateral sections of the eye allows for greater light sensitivity and may improve the likelihood of snow crab seeing dimly lit pots or other objects from the side. This peripheral light sensitivity is analogous to human vision when a dim object, such as a star, is only visible while focused away from it; the densely packed cones in the fovea centralis (focal point on the retina) are not as light-sensitive as the rods in the periphery, allowing human peripheral vision to be better at seeing dim objects in low-light conditions [64].



Figure 10. The image on the left is a snow crab pseudopupil from the eye's dorsal facing area when the eye is in the orbital space, scanning above. It is posterolateral facing when elevated, scanning the horizon. The image on the right is of the same location on the eye but was taken at 50× magnification under a dissecting microscope, showing the large ommatidial facets.

Supporting these acuity results is the pseudopupil shape (Figures 9 and 10). The pseudopupil in compound eyes appears as if a pupil follows the viewer as they move. The pseudopupil, however, is an illusion where the viewer observes the absence of a reflection (black and pupil-like) from the ommatidia that absorb light from the viewer's position. The pseudopupil of snow crab is largest across the center, rectangle-shaped, and several dozen ommatidia wide, stretching from the distal to the proximal end of the eye (Figure 9). As the viewer orients from the front to the rear-facing portion of the snow crab eye, the rectangular pseudopupil follows without changing shape until near the edges of the ommatidia (personal observations). When the viewer orients from a proximal or distal position, there is only a thin pseudopupil around the edges of the eye. The large pseudopupil of snow crab supports the idea that they have relatively high visual acuity for compound eyes. The vertical orientation of the pseudopupil also reinforces the discussion above about the possible vertical resolving power of snow crab.

The distal portion of the eye appears to have screening pigments that fade dorsoventrally (Figure 9), as seen in fiddler crabs [65], suggesting that these screening pigments protect their eyes from stray light. These screening pigments could also allow for a degree of color discrimination in the dorsal part of the eye.

4.5. Reduced Light Sensitivity in Damaged Eyes

Crustaceans removed rapidly from darker environments (i.e., deep water) have shown signs of severe damage to their visual components [66]. Before being discarded in commercial snow crab fisheries, sub-legal male, female, and softshell male crab are exposed to intense light and often higher temperatures, significantly increasing their risk of eye damage [67]. Damage to the eyes can cause behavioral changes that reduce survival and reproductive success [66,68]. The damage would also reduce the snow crab's ability to detect the dim light from phosphorescent-netting pots, meaning that those crab that had not been previously discarded may see the light from a greater distance. Those crab that are removed from deeper, and thus darker, environments would be the most at risk for potentially irreversible light-induced damage [69,70], even if only exposed to sunlight for less than 1 min [71].

4.6. Knowledge Gaps

Although small males and females were not sampled in this study, it is reasonable to assume that their eyes are also smaller and, therefore, their visual acuity and sensitivity are worse [72]. Smaller eyes of the same crustacean species have larger interommatidial angles and shorter focal lengths, leading to lower spatial resolution [60,72]. Smaller eyes also have narrower apertures for collecting light, causing them to be less light-sensitive than larger eyes [72]. Given this information, we can assume that phosphorescent-netting pots may be visible at greater distances for larger snow crab, especially during initial deployment when light intensity and contrast are at their highest.

Visual acuity was estimated using local radius curvature measurements from a 2-dimensional image of snow crab eyes, and only on the vertical axis. However, the eye is 3-dimensional, and more accurate measurements would entail an average of local radii from multiple angles. Thus, visual acuity is likely slightly overestimated in some regions and underestimated in others because of this measurement technique.

We may also be overestimating visual acuity, because there are many adaptations that crustaceans could make to their dim environment, including spatial summation (neural pooling) and temporal summation [22,73]. Neural pooling is when information from multiple adjacent ommatidia provide information as a single summation, increasing sensitivity but decreasing resolution [73]. Snow crab may also have a high degree of temporal summation. Temporal summation is an increase in integration time for visual signals, where ommatidia absorb photons for a period of time before sending a signal [22,73]. This buffering allows more photon collection and stronger signals where there is light. High temporal summation reduces temporal resolution but not necessarily visual acuity. However, even a slight movement of the snow crab or its environment would decrease visual acuity in this situation [73]. These characteristics would be helpful in some deepwater species where light is limited, but they have trade-offs that limit vision in other aspects; e.g., high temporal summation reduces the likelihood of seeing flashing bioluminescence or moving objects [71,73]. Because there are no studies on the visual capacity of snow crab, we cannot be sure if either of these traits are present or absent. Future research into the visual capacity of snow crab would greatly benefit from additional anatomical and physiological eye studies. Theoretical sensitivity limits could be derived in future research with additional morphological measurements (e.g., photoreceptor size, rhabdom width), although integration time would have to be assumed using this approach [74,75].

To determine the importance of nighttime fishing of the phosphorescent-netting pots and to validate the decay rate of the model, temperature-appropriate measurements of the light emitted from pots beyond one hour are needed. Additionally, solar irradiance measurements throughout the day and night are needed to ensure accuracy for determining whether the contrast model results are appropriate, particularly when predicting well beyond the measured data.

To our knowledge, this is one of the first published studies on the physical characteristics of snow crab eyes (see Meyers et al. [24]) and the first that estimates their visual

capacity. Because of this lack of information on snow crab vision, we must either make assumptions or ignore factors that may affect the models. Additional research that would help inform the understanding of snow crab vision would include but is not limited to understanding the presence or degree of size/sex dependence on visual characteristics, temporal summation, neural superposition, screening pigments, polarization vision, opsin characterization and spectral sensitivity, contrast sensitivity, and dark- vs. light-adapted characteristics. Knowing how snow crab use posturing and eye movement to view their environment would also be beneficial.

Future research into contrast sensitivity could also help us understand how snow crab perceive traditional pots. Because traditional pots have orange, red, or black twine and are 200 m deep in the ocean, pots are likely prominent silhouettes to snow crab during the day, as they would appear dark black against the ambient light. The brighter the ambient light, the higher the contrast of the pots. Thus, at 200 m, snow crab likely use their vision to assist in the capture process during daylight hours with traditional pots. At night, bioluminescent animals may interact with or be near the pot and aid in the capture process. However, in the absence of bioluminescent animals, the crab's other senses are likely used in capture at night. Perhaps phosphorescent-netting pots increase the visual-system-associated fishing effort from daylight hours to day and night. In that respect, if smaller snow crab are more risk-averse and forage at night more often [76], they may encounter phosphorescent-netting pots more frequently than traditional pots. Conversely, studies show that adult male snow crab move a greater distance than juvenile males and females, increasing their likelihood of encountering and interacting with the light from phosphorescent-netting pots [76–78]. These are all speculations on snow crab's visual ecology and behavior but could be clarified with additional research into their visual capabilities.

5. Conclusions

The models in this study could predict how other animals perceive their environment, phosphorescent-netting pots, and other light sources. Parameter values and the model itself would need to be adjusted according to life history (depth, diurnal movement, etc.), typical environment, viewing angle, spectral sensitivity, contrast threshold, light-source size, and visual acuity. Depending on the species and location, additional factors may be needed. Light source characteristics should be heavily considered when pursuing the potential visual perception of animals in fisheries using light, as we have done with phosphorescent-netting pots. This information would help us understand the potential impact of light technology on the behavior of non-target animals in the vicinity, particularly at night or in darker environments. This approach provides a path forward in gear innovation while being cognizant of the possible effects on the local environment.

Supplementary Materials: The following supporting information can be downloaded at: <https://www.mdpi.com/article/10.3390/fishes9050185/s1>.

Author Contributions: Conceptualization, C.F., S.B. and P.-P.B.; methodology, C.F., S.B. and P.-P.B.; software, P.-P.B.; validation, C.F., S.B. and P.-P.B.; formal analysis, C.F. and P.-P.B.; investigation, C.F. and R.S.; resources, S.B. and P.-P.B.; data curation, C.F., R.S. and P.-P.B.; writing—original draft preparation, C.F.; writing—review and editing, S.B., R.S. and P.-P.B.; visualization, C.F. and S.B.; supervision, S.B. and P.-P.B.; project administration, S.B.; funding acquisition, S.B. All authors have read and agreed to the published version of the manuscript.

Funding: This research was funded by an Ocean Frontier Institute Seed Fund, SnowMap, NSERC Discovery Grant 201904984 awarded to P.-P.B., and NSERC Discovery Grant 202103248 awarded to S.B.

Institutional Review Board Statement: Not applicable.

Informed Consent Statement: Not applicable.

Data Availability Statement: The data presented in this study are available on request from the corresponding author.

Acknowledgments: The authors would like to thank those that contributed to this work, including Pedro Sa (Euronete), Jerry Williams (ESL Marine Supplies Ltd.), Meghan Donovan (Centre for Fisheries Ecosystems Research), and Paul Winger (Centre for Sustainable Aquatic Resources). Additional thanks to Eleanor Caves (University of California Santa Barbara), Tomas Araya-Schmidt (Centre for Sustainable Aquatic Resources), and Kristine Cerbule (University of Tromsø—The Arctic University of Norway).

Conflicts of Interest: The authors declare that there are no conflicts of interest.

Appendix A

1. SACALC 3.14 software settings.

Source Dimensions: source radius: $r_1 = 60$, source thickness: $t_1 = 0$

Detector Dimensions: detector radius: $r_2 = 1.95$, detector thickness: $t_2 = 0$

Detector–Source Displacement: displacement: $d = 0$, displacement: $c =$ each recorded distance from detector to disc

Rotational Angles: $x = 0$, $y = 0$, $z = 0$

Source Emissions: 2π source, Emissions = 1×10^7

2. SMARTS v2.9.5 code settings

Location: Port de Grave, NL (47.585, -53.213)

Date: 18 April 2022 (first day of fishing season)

Time: 12:00

Angle of Surface: Horizontal (not tilted: tangent to earth's surface)

Solar Zenith: 44.71

CO₂: 412.0 ppm (measurement as of 18 April 2022)

Aerosol: S&F maritime [79]

Turbidity: TAU5 (aerosol optical depth at 500 nm, t_5) = 0.084 (default)

References

1. FFA. Seafood Industry Year in Review 2022. Newfoundland and Labrador Canada. Fisheries, Forestry, and Agriculture. 2023. Available online: <https://www.gov.nl.ca/ffa/files/Seafood-Industry-Year-in-Review-2022.pdf> (accessed on 10 May 2024).
2. Mallowney, D.R.J.; Baker, K.D.; Pantin, J.R. Hard to manage? Dynamics of soft-shell crab in the Newfoundland and Labrador snow crab fishery. *Front. Mar. Sci.* **2021**, *8*, 591496. [CrossRef]
3. DFO. Assessment of Newfoundland and Labrador (Divisions 2HJ3KLKNOP4R) Snow Crab. Canadian Science Advisory Secretariat, Science Advisory Report 2022/012. 2022. Available online: https://publications.gc.ca/collections/collection_2022/mpo-dfo/fs70-6/Fs70-6-2022-012-eng.pdf (accessed on 10 May 2024).
4. Nguyen, K.Q.; Winger, P.D. Artificial light in commercial industrialized fishing applications: A review. *Rev. Fish. Sci. Aquac.* **2019**, *27*, 106–126. [CrossRef]
5. Mallowney, D.R.J.; Baker, K.D.; Pedersen, E.J. Harvesting strategies during a forecasted decline in the Newfoundland and Labrador snow crab fishery. *Fish. Res.* **2020**, *232*, 105707. [CrossRef]
6. Olsen, L.; Herrmann, B.; Sistiaga, M.; Grimaldo, E. Effect of gear soak time on size selection in the snow crab pot fishery. *Fish. Res.* **2019**, *214*, 157–165. [CrossRef]
7. Nguyen, K.Q.; Winger, P.D.; Morris, C.; Grant, S.M. Artificial lights improve the catchability of snow crab (*Chionoecetes opilio*) traps. *Aquac. Fish.* **2017**, *2*, 124–133. [CrossRef]
8. Olsen, L.; Herrmann, B.; Grimaldo, E.; Sistiaga, M. Effect of pot design on the catch efficiency of snow crabs (*Chionoecetes opilio*) in the Barents Sea fishery. *PLoS ONE* **2019**, *14*, e0219858. [CrossRef]
9. Cerbule, K.; Herrmann, B.; Grimaldo, E.; Sistiaga, M.; Brinkhof, J.; Vollstad, J. Understanding and predicting the effect of entrance cone diameters on the catch efficiency of snow crabs (*Chionoecetes opilio*) in conical pots. *Reg. Stud. Mar. Sci.* **2022**, *52*, 102237. [CrossRef]
10. Winger, P.D.; Walsh, P.J. Selectivity, efficiency, and underwater observations of modified trap designs for the snow crab (*Chionoecetes opilio*) fishery in Newfoundland and Labrador. *Fish. Res.* **2011**, *109*, 107–113. [CrossRef]
11. Anders, N.; Ingólfsson, Ó.A.; Jørgensen, T.; Løkkeborg, S.; Humborstad, O.-B. Investigating the potential of escape openings and reduced mesh size to optimize snow crab (*Chionoecetes opilio*) pot catches in the Barents Sea. *Fish. Res.* **2023**, *258*, 106517. [CrossRef]
12. Weissburg, M.J.; Zimmer-Faust, R.K. Odor plumes and how blue crabs use them in finding prey. *J. Exp. Biol.* **1994**, *197*, 349–375. [CrossRef]
13. Zimmer-Faust, R.K.; Finelli, C.M.; Pentcheff, N.D.; Wethey, D.S. Odor Plumes and Animal Navigation in Turbulent Water Flow: A Field Study. *Bio Bull.* **1995**, *188*, 111–116. [CrossRef] [PubMed]

14. Nguyen, K.Q.; Winger, P.D.; Wood, J.; Donovan, M.; Humborstad, O.-B.; Lokkeborg, S.; Bayse, S.M. Application of luminescent netting in traps to improve the catchability of the snow crab *Chionoecetes opilio*. *Mar. Coast. Fish. Dyn. Manag. Ecosyst. Sci.* **2019**, *11*, 295–304. [CrossRef]
15. Anesh, M.P.; Gulrez, S.K.H.; Anis, A.; Shaikh, H.; Ali Mohsin, M.E.; AL-Zahrani, S.M. Developments in Eu+2-doped strontium aluminate and polymer/strontium aluminate composite. *Adv. Polym. Technol.* **2014**, *33*, 21436. [CrossRef]
16. Matsuzawa, T.; Aoki, Y.; Takeuchi, N.; Murayama, Y. A New Long Phosphorescent Phosphor with High Brightness, SrAl₂O₄:Eu²⁺, Dy³⁺. *J. Electrochem. Soc.* **1996**, *143*, 2670. [CrossRef]
17. Fouzar, S.; Eftimov, T.; Kostova, I.; Benmounah, A.; Lakhssassi, A. Effects of temperature on the time responses of strontium aluminates. *Opt. Mater.* **2021**, *122*, 111619. [CrossRef]
18. Rojas-Hernandez, R.E.; Rubio-Marcos, F.; Rodriguez, M.A.; Fernandez, J.F. Long lasting phosphors: SrAl₂O₄:Eu, Dy as the most studied material. *Renew. Sustain. Energy Rev.* **2018**, *81*, 2759–2770. [CrossRef]
19. Aas, E.; Højerslev, N.K.; Høkedal, J.; Sørensen, K. Optical water types of the Nordic Seas and adjacent areas. *Oceanologia* **2013**, *55*, 471–482. [CrossRef]
20. Cronin, T.W.; Johnsen, S.; Marshall, N.J.; Warrant, E.J. *Visual Ecology*; Princeton University Press: Princeton, NJ, USA, 2014; Available online: <http://www.jstor.org/stable/j.ctt6wq1c9> (accessed on 10 May 2024).
21. Jerlov, N.G. Irradiance optical classification. In *Optical Oceanography*; American Elsevier Publishing Co.: New York, NY, USA, 1968; pp. 118–120. [CrossRef]
22. Caves, E.M.; Frank, T.M.; Johnsen, S. Spectral sensitivity, spatial resolution and temporal resolution and their implications for conspecific signalling in cleaner shrimp. *J. Exp. Biol.* **2016**, *219*, 597–608. [CrossRef]
23. Cronin, T.W.; Forward, R.B. The visual pigments of crabs. *J. Comp. Physiol. A* **1988**, *162*, 463–478. [CrossRef]
24. Meyers, T.R.; Morris, R.; Jackson, T.M.; Dissen, J.N.; Slater, L.M.; Groner, M.L. Black eye syndrome and a systemic rickettsia-like organism in Alaskan *Chionoecetes* spp. crabs, including normal eyestalk microanatomy. *Dis. Aquat. Org.* **2022**, *150*, 103–124. [CrossRef]
25. R Core Team. *R: A Language and Environment for Statistical Computing*; R Foundation for Statistical Computing: Vienna, Austria, 2022; Available online: <https://www.R-project.org/> (accessed on 10 May 2024).
26. Maia, R.; Gruson, H.; Endler, J.A.; White, T.E. pavo 2: New tools for the spectral and spatial analysis of colour in R. *Methods Ecol. Evol.* **2019**, *10*, 1097–1107. [CrossRef]
27. Johnsen, S. *The Optics of Life: A Biologist's Guide to Light in Nature*; Princeton University Press: Princeton, NJ, USA, 2012; Available online: <http://www.jstor.org/stable/j.ctt7s4q4> (accessed on 10 May 2024).
28. Whitcher, R. SACALC3; OECD. Nuclear Energy Agency Data Bank: Issy-Les Moulineaux, France, 2012.
29. Eftimov, T.; Kostova, I.; Arapova, A.; Patronov, G. Rise and decay time responses of Sr aluminate phosphorescent materials. *J. Lumin.* **2021**, *235*, 117985. [CrossRef]
30. Schneider, C.A.; Rasband, W.S.; Eliceiri, K.W. NIH Image to ImageJ: 25 years of image analysis. *Nat. Methods* **2012**, *9*, 671–675. [CrossRef] [PubMed]
31. Baldwin-Fergus, J.L.; Johnsen, S.; Osborn, K.J. A unique apposition compound eye in the mesopelagic hyperiid amphipod *Paraphronima gracilis*. *Curr. Biol.* **2015**, *25*, 473–478. [CrossRef] [PubMed]
32. Land, M.F.; Nilsson, D.-E. *Animal Eyes*, 2nd ed.; Oxford University Press: Oxford, UK, 2012. [CrossRef]
33. Feller, K.D.; Sharkey, C.R.; McDuffee-Altekruse, A.; Bracken-Grissom, H.D.; Lord, N.P.; Porter, M.L.; Schweikert, L.E. Surf and turf vision: Patterns and predictors of visual acuity in compound eye evolution. *Arthropod Struct. Dev.* **2021**, *60*, 101002. [CrossRef] [PubMed]
34. Nilsson, D.-E.; Ro, A.-I. Did neural pooling for night vision lead to the evolution of neural superposition eyes? *J. Comp. Physiol. A* **1994**, *175*, 289–302. [CrossRef]
35. Caves, E.M.; Johnsen, S. AcuityView: An r package for portraying the effects of visual acuity on scenes observed by an animal. *Methods Ecol. Evol.* **2018**, *9*, 793–797. [CrossRef]
36. Marshall, J.; Kent, J.; Cronin, T. Visual adaptations in crustaceans: Spectral sensitivity in diverse habitats. In *Adaptive Mechanisms in the Ecology of Vision*; Archer, S.N., Djamgoz, M.B.A., Loew, E.R., Partridge, J.C., Vallerga, S., Eds.; Springer: Dordrecht, The Netherlands, 1999; pp. 285–327. [CrossRef]
37. Marshall, J.N.; Cronin, T.W.; Frank, T.M. Visual adaptations in crustaceans: Chromatic, developmental, and temporal aspects. In *Sensory Processing in Aquatic Environments*; Collin, S.P., Marshall, N.J., Eds.; Springer: New York, NY, USA, 2003; pp. 343–372. [CrossRef]
38. Dawis, S.M. Polynomial expressions of pigment nomograms. *Vis. Res.* **1981**, *21*, 1427–1430. [CrossRef]
39. Dartnall, H.J.A. The interpretation of spectral sensitivity curves. *Br. Med. Bull.* **1953**, *9*, 24–30. [CrossRef]
40. Drerup, C.; How, M.J. Polarization contrasts and their effect on the gaze stabilization of crustaceans. *J. Exp. Biol.* **2021**, *224*, jeb229898. [CrossRef]
41. Douglas, R.H.; Hawryshyn, C.W. Behavioural studies of fish vision: An analysis of visual capabilities. In *The Visual System of Fish*; Douglas, R.H., Djamgoz, M.B.A., Eds.; Springer: Dordrecht, The Netherlands, 1990; pp. 373–418.
42. Solonenko, M.G.; Mobley, C.D. Inherent optical properties of Jerlov water types. *Appl. Opt.* **2015**, *54*, 5392–5401. [CrossRef] [PubMed]

43. Partridge, J.C. The colour sensitivity and vision of fishes. In *Light and Life in the Sea*; Herring, P.J., Campbell, A.K., Whitfield, M., Maddock, L., Eds.; Cambridge University Press: Cambridge, UK, 1990; pp. 167–184.
44. Santon, M.; Bitton, P.-P.; Dehm, J.; Fritsch, R.; Harant, U.K.; Anthes, N.; Michiels, N.K. Redirection of ambient light improves predator detection in a diurnal fish. *Proc. R. Soc. B Biol. Sci.* **2020**, *287*, 20192292. [[CrossRef](#)] [[PubMed](#)]
45. Pepin, P.; Maillet, G.; Fraser, S.; Doyle, G.; Robar, A.; Shears, T.; Redmond, G. Optical, Chemical, and Biological Oceanographic Conditions on the Newfoundland and Labrador Shelf during 2014–2015. Fisheries and Oceans Canada, Science Branch. Research Document: 2017/009. 2017. Available online: <https://waves-vagues.dfo-mpo.gc.ca/library-bibliotheque/40601845.pdf> (accessed on 10 May 2024).
46. Nilsson, D.-E.; Warrant, E.; Johnsen, S. Computational visual ecology in the pelagic realm. *Philos. Trans. R. Soc. B* **2014**, *369*, 20130038. [[CrossRef](#)] [[PubMed](#)]
47. Johnsen, S.; Widder, E.A.; Mobley, C.D. Propagation and perception of bioluminescence: Factors affecting counterillumination as a cryptic strategy. *Bio. Bull.* **2004**, *207*, 1–16. [[CrossRef](#)] [[PubMed](#)]
48. Gueymard, C.A. The SMARTS spectral irradiance model after 25 years: New developments and validation of reference spectra. *Sol. Energy* **2019**, *187*, 233–253. [[CrossRef](#)]
49. Sathyendranath, S.; Platt, T. The light field in the ocean: Its modification and exploitation by the pelagic biota. In *Light and Life in the Sea*; Herring, P.J., Campbell, A.K., Whitfield, M., Maddock, L., Eds.; Cambridge University Press: Cambridge, UK, 1990; pp. 3–18.
50. Loew, E.R.; McFarland, W.N. The underwater visual environment. In *The Visual System of Fish*; Douglas, R.H., Djamgoz, M.B.A., Eds.; Springer: Dordrecht, The Netherlands, 1990; pp. 1–43.
51. Nicol, J.A.C. The photoenvironment. In *The Eyes of Fishes*; Oxford University Press: Oxford, UK, 1989; pp. 4–16.
52. Doujak, F.E. Can a shore crab see a star? *J. Exp. Biol.* **1985**, *116*, 385–393. [[CrossRef](#)]
53. Mishra, S.B.; Mishra, A.K.; Revaprasadu, N.; Hillie, K.T.; Steyn, W.J.v.; Coetsee, E.; Swart, H.C. Strontium aluminate/polymer composites: Morphology, luminescent properties, and durability. *J. Appl. Polym. Sci.* **2009**, *112*, 3347–3354. [[CrossRef](#)]
54. Ge, M.; Guo, X.; Yan, Y. Preparation and study on the structure and properties of rare-earth luminescent fiber. *Text. Res. J.* **2012**, *82*, 677–684. [[CrossRef](#)]
55. Frank, C.C.H.; Bayse, S.M. The effect of variable light intensity in luminescent-netting pots on the catch of snow crab (*Chionoectes opilio*). *Aquac. Fish.* **2023**; *in press*. [[CrossRef](#)]
56. Burrows, M.; Horridge, G.A. Eyecup withdrawal in the crab, *Carcinus*, and its interaction with the optokinetic response. *J. Exp. Biol.* **1968**, *49*, 285–297. [[CrossRef](#)]
57. Su, T.L.; Lim, S.L. To flee or not to flee: Characterising differentiated anti-predatory responses of two mangrove crabs. *Ethol. Ecol. Evol.* **2015**, *29*, 181–192. [[CrossRef](#)]
58. Conan, G.Y.; Starr, M.; Comeau, M.; Therriault, J.-C.; Hernandez, F.X.M.; Robichaud, G. Life history strategies, recruitment fluctuations, and management of the Bonne bay fjord Atlantic snow crab (*Chionoectes opilio*). In *High Latitude Crabs: Biology, Management, and Economics*; Alaska Sea Grant: Anchorage, AK, USA, 1996; pp. 59–97.
59. Ottmar, M.L.; Ryer, C.H.; Hurst, T.P. Comparative predator-mediated habitat use in early juvenile southern Tanner crab (*Chionoectes bairdi*), snow crab (*Chionoectes opilio*), and red king crab (*Paralithodes camtschaticus*). *J. Exp. Mar. Biol. Ecol.* **2022**, *555*, 151792. [[CrossRef](#)]
60. Hiller-Adams, P.; Case, J.F. Eye size of pelagic crustaceans as a function of habitat depth and possession of photophores. *Vis. Res.* **1988**, *28*, 667–680. [[CrossRef](#)]
61. Nalbach, H.-O. Multisensory control of eyestalk orientation in decapod crustaceans: An ecological approach. *J. Crustac. Biol.* **1990**, *10*, 382–399. [[CrossRef](#)]
62. Smolka, J.; Hemmi, J.M. Topography of vision and behaviour. *J. Exp. Biol.* **2009**, *212*, 3522–3532. [[CrossRef](#)] [[PubMed](#)]
63. Mullaney, D.R.J.; Dawe, E.; Colbourne, E.B.; Rose, G.A. A review of factors contributing to the decline of Newfoundland and Labrador snow crab (*Chionoectes opilio*). *Rev. Fish Biol. Fish.* **2014**, *24*, 639–657. [[CrossRef](#)]
64. Tuten, W.S.; Harmening, W.M. Foveal vision. *Curr. Biol.* **2021**, *31*, R701–R703. [[CrossRef](#)] [[PubMed](#)]
65. Zeil, J.; Hemmi, J.M. The visual ecology of fiddler crabs. *J. Comp. Physiol. A* **2006**, *192*, 1–25. [[CrossRef](#)]
66. Meyer-Rochow, V.B. The crustacean eye: Dark/light adaptation, polarization sensitivity, flicker fusion frequency, and photoreceptor damage. *Zool. Sci.* **2001**, *18*, 1175–1197. [[CrossRef](#)]
67. Kashiwagi, T.; Meyer-Rochow, V.B.; Nishimura, K.; Eguchi, E. Fatty acid composition and ultrastructure of photoreceptive membranes in the crayfish *Procambarus clarkii* under conditions of thermal and photic stress. *J. Comp. Physiol. B* **1997**, *167*, 1–8. [[CrossRef](#)]
68. Meyer-Rochow, V.B. Light-induced damage to the photoreceptors of spiny lobsters and other crustaceans. *Crustaceana* **1994**, *67*, 95–109. [[CrossRef](#)]
69. Gaten, E. Optics and phylogeny: Is there insight? The evolution of superposition eyes in Decapoda (Crustacea). *Contrib. Zool.* **1998**, *67*, 223–235. [[CrossRef](#)]
70. Herring, P.J.; Campbell, A.K.; Whitfield, M.; Maddock, L. *Light and Life in the Sea*; Cambridge University Press: Cambridge, UK, 1990.
71. Frank, T.M.; Johnsen, S.; Cronin, T.W. Light and vision in the deep-sea benthos: II. Vision in deep-sea crustaceans. *J. Exp. Biol.* **2012**, *215*, 3344–3353. [[CrossRef](#)] [[PubMed](#)]

72. Schweikert, L.E.; Thomas, K.N.; Moreno, V.M.; Casaubon, A.; Golightly, C.; Bracken-Grissom, H.D. Ecological predictors and functional implications of eye size in deep-sea shrimps. *Front. Ecol. Evol.* **2022**, *10*, 787315. [[CrossRef](#)]
73. Bagheri, Z.M.; Jessop, A.-L.; Partridge, J.C.; Osborn, K.J.; Hemmi, J.M. A new computational model illuminates the extraordinary eyes of *Phronima*. *PLoS Comput. Biol.* **2022**, *18*, e1010545. [[CrossRef](#)] [[PubMed](#)]
74. Schweikert, L.E.; Davis, A.L.; Johnsen, S.; Bracken-Grissom, H.D. Visual perception of light organ patterns in deep-sea shrimps and implications for conspecific recognition. *Ecol. Evol.* **2020**, *10*, 9503–9513. [[CrossRef](#)] [[PubMed](#)]
75. Warrant, E.J. Seeing better at night: Life style, eye design and the optimum strategy of spatial and temporal summation. *Vis. Res.* **1999**, *39*, 1611–1630. [[CrossRef](#)]
76. Cote, D.; Nicolas, J.-M.; Whoriskey, F.; Cook, A.M.; Broome, J.; Regular, P.M.; Baker, D. Characterizing snow crab (*Chionoecetes opilio*) movements in the Sydney Bight (Nova Scotia, Canada): A collaborative approach using multiscale acoustic telemetry. *Can. J. Fish. Aquat. Sci.* **2018**, *76*, 334–346. [[CrossRef](#)]
77. Florko, K.R.N.; Davidson, E.R.; Lees, K.J.; Hammer, L.J.; Lavoie, M.-F.; Lennox, R.J.; Simard, E.; Archambault, P.; Auger-Methe, M.; McKindsey, C.W.; et al. Tracking movements of decapod crustaceans: A review of a half-century of telemetry-based studies. *Mar. Ecol. Prog. Ser.* **2021**, *679*, 219–239. [[CrossRef](#)]
78. Maynard, D.R.; Robichaud, D.A. *Short Term Movements of Snow Crabs (Chionoecetes opilio) in Bay of Islands, Newfoundland, as Monitored by Ultrasonic Trackings*; Research Document: 86/50; Department of Fisheries and Oceans, Canadian Atlantic Fisheries Scientific Advisory Committee: Dartmouth, NS, Canada, 1986.
79. Shettle, E.P.; Fenn, R.W. Models for the Aerosols of the Lower Atmosphere and the Effects of Humidity Variations on Their Optical Properties. Optical Physics Division, Air Force Geophysics Laboratory, Environmental Research Papers No. 676. 1979. Available online: <https://apps.dtic.mil/sti/citations/ADA085951> (accessed on 10 May 2024).

Disclaimer/Publisher’s Note: The statements, opinions and data contained in all publications are solely those of the individual author(s) and contributor(s) and not of MDPI and/or the editor(s). MDPI and/or the editor(s) disclaim responsibility for any injury to people or property resulting from any ideas, methods, instructions or products referred to in the content.